The EMBO Journal (2007) 26, 2192–2205 | © 2007 European Molecular Biology Organization | All Rights Reserved 0261-4189/07
www.embojournal.org

THE EMBO JOURNAL

Crystal structures of autoinhibitory PDZ domain of Tamalin: implications for metabotropic glutamate receptor trafficking regulation

Takuma Sugi[1,4], Takuji Oyama[2,4], Takanori Muto[1,5], Shigetada Nakanishi[3], Kosuke Morikawa[2,4,*] and Hisato Jingami[1,6,*]

[1]Department of Molecular Biology, Biomolecular Engineering Research Institute (BERI), Suita, Osaka, Japan, [2]Department of Structural Biology, Biomolecular Engineering Research Institute (BERI), Suita, Osaka, Japan and [3]Department of Systems Biology, Osaka Bioscience Institute, Osaka, Japan

Metabotropic glutamate receptors (mGluRs) function as neuronal G-protein-coupled receptors and this requires efficient membrane targeting through associations with cytoplasmic proteins. However, the molecular mechanism regulating mGluR cell-surface trafficking remains unknown. We report here that mGluR trafficking is controlled by the autoregulatory assembly of a scaffold protein Tamalin. In the absence of mGluR, Tamalin self-assembles into autoinhibited conformations, through its PDZ domain and C-terminal intrinsic ligand motif. X-ray crystallographic analyses visualized integral parts of the oligomeric self-assemblies of Tamalin, which require not only the novel hydrophobic dimerization interface but also canonical and noncanonical PDZ/ligand autoinhibitory interactions. The mGluR cytoplasmic region can competitively bind to Tamalin at a higher concentration, disrupting weak inhibitory interactions. The atomic view of mGluR association suggests that this rearrangement is dominated by electrostatic attraction and repulsion. We also observed in mammalian cells that the association liberates the intrinsic ligand toward a motor protein receptor, thereby facilitating mGluR cell-surface trafficking. Our study suggests a novel regulatory mechanism of the PDZ domain, by which Tamalin switches between the trafficking-inhibited and -active forms depending on mGluR association.

*Corresponding authors. H Jingami, Office of Graduate Courses for Integrated Research Training, Kyoto University, Yoshida-Konoe, Sakyo-Ku, Kyoto 606-8501, Japan. Tel.: +81 75 753 9493; Fax: +81 75 753 9495. E-mail: jingami@mfour.med.kyoto-u.ac.jp or K Morikawa, Institute for Protein Research, Open Laboratories of Advanced Bioscience and Biotechnology (OLABB), Osaka University, 6-2-3, Furuedai, Suita, Osaka 565-0874, Japan. Tel.: +81 6 6872 8201; Fax: +81 6 6872 19. E-mail: morikako@protein.osaka-u.ac.jp
[4]Present address: Institute for Protein Research, Open Laboratories of Advanced Bioscience and Biotechnology (OLABB), Osaka University, 6-2-3, Furuedai, Suita, Osaka 565-0874, Japan
[5]Present address: Fuji Gotemba Research Laboratories, Chugai Pharmaceutical Co., Ltd, 1-135 Komakado, Gotemba, Shizuoka 412-8513, Japan
[6]Present address: Office of Graduate Courses for Integrated Research Training, Kyoto University Faculty of Medicine, Yoshida, Sakyo-Ku, Kyoto 606-8501, Japan

Received: 6 October 2006; accepted: 23 February 2007; published online: 29 March 2007

The EMBO Journal (2007) **26,** 2192–2205. doi:10.1038/sj.emboj.7601651; Published online 29 March 2007
Subject Categories: membranes & transport; structural biology
Keywords: autoinhibited assembly; metabotropic glutamate receptor; PDZ domain; Tamalin; trafficking

Introduction

Proper spatio-temporal organization of diverse proteins at the postsynaptic density is critical for effective synaptic neurotransmission (Kennedy, 2000). Ionotropic (iGluRs) and metabotropic (mGluRs) glutamate receptors are highly organized components of protein interaction networks. Previous reports on iGluR organization described various scaffold proteins that dynamically assemble iGluRs into downstream signaling proteins and target their complexes to specific subcellular locations through multiple modular domains (Li and Sheng, 2003). By contrast, proteins with analogous functions have not been investigated thoroughly, in terms of mGluR organization. mGluRs are class III/C G-protein-coupled receptors (GPCRs) that mediate slow excitatory synaptic transmission by transmitting glutamate stimulation to second messenger cascades via G-proteins. Although recent studies suggested that signaling by mGluRs depends on their cellular organization through associations with various proteins, such as Homer, Calmodulin and Seven in absentia homologue (Hall and Lefkowitz 2002; Fagni *et al*, 2004), the underlying regulatory mechanisms of molecular scaffolding still remain to be elucidated.

Tamalin, which is also called the GRP1-associated scaffold protein (Nevrivy *et al*, 2000), is developmentally expressed mainly in the brain telencephalic region (Kitano *et al*, 2002). Recent studies have revealed that Tamalin functions as a molecular scaffold that links receptors, including group I mGluRs (mGluR1 and mGluR5), to multiple neuronal proteins. For example, an ITAM motif in the N-terminal alanine-rich (AR) region is phosphorylated by Src kinase, depending on the interaction with mGluRs, which then recruits Syk kinase and activates a signaling cascade (Hirose *et al*, 2004). Furthermore, a recent study revealed a new signaling pathway, in which Tamalin links a kinase-deficient neurotrophin receptor isoform, TrkCT1, to the Arf6/Rac1 signaling, in a neurotrophin-dependent manner (Esteban *et al*, 2006). The neurotrophin stimulation causes actin reorganization and membrane ruffling.

In addition to these signaling complexes, Tamalin forms a protein complex with group I mGluRs and cytohesin 2, a guanine nucleotide exchange factor, through the PDZ domain and the Leu-zipper region, respectively (Kitano *et al*, 2002). In triply transfected COS-7 cells and cultured

hippocampal neurons, Tamalin and its mutant lacking the Leu-zipper increased and reduced the membranous trafficking of mGluRs, respectively. Yet, importantly, the Tamalin PDZ domain also possesses an ability to associate with its conserved C-terminal PDZ-binding motif (Kitano *et al*, 2003). Moreover, this motif interacts with another PDZ scaffold protein, S-SCAM, *in vivo* (Kitano *et al*, 2003), which functions as the receptor for a molecular motor, linking cargo receptors to the kinesin superfamily motor protein (Mok *et al*, 2002). This situation may require more intricate molecular mechanisms, and thus raises the question of how Tamalin distinguishes between its own and the mGluR C-terminal tail. Although recent structural analyses of other PDZ proteins have clarified the recognition modes for their respective ligands, little is known about how the single PDZ domain discriminates between its multiple relevant targets and what effects are provided by binding partner exchange (Hung and Sheng, 2002). The importance of the target discrimination has been highlighted by the fact that the Dishevelled PDZ domain distinguishes between the canonical and noncanonical Wnt signaling pathways, depending on the affinity differences between its binding partners (Wong *et al*, 2003). These studies tempted us to postulate that the structural discrimination between the Tamalin C-terminus, that is, 'intrinsic ligand', and the mGluR C-terminus by the PDZ domain would be critical for mGluR cell-surface trafficking.

Here, we present a molecular mechanism of mGluR trafficking regulation by Tamalin. Biochemical assays revealed that Tamalin forms autoinhibited assemblies through its PDZ domain and intrinsic ligand until it becomes bound to mGluRs. We illustrated a core part of these assemblies by X-ray crystallographic analyses. The mGluR cytoplasmic region can disrupt the self-assembly of Tamalin to relieve its intrinsic ligand for S-SCAM, thereby processing cell-surface trafficking. Thus, Tamalin changes its trafficking activity between the autoinhibited and released states in an mGluR concentration-dependent manner.

Results

Autoregulatory role for the Tamalin C-terminal intrinsic ligand in mGluR cell-surface trafficking

To examine the functional role of the intrinsic ligand of Tamalin, we first compared the effects of the full-length and intrinsic ligand-deficient forms of Tamalin on the cell-surface expression of mGluR in COS-7 cells, by a surface protein biotinylation assay. We confirmed that no cytoplasmic cytohesin 2 was recovered under the experimental conditions (data not shown), indicating that the membrane surface receptors were specifically obtained. As previously reported (Kitano *et al*, 2002), we observed that the deletion of the C-terminal 234 residues of mGluR1α significantly reduced its surface expression, and thus mGluR1α cell-surface expression depends on its specific interaction with Tamalin (Figure 1A and B).

Figure 1C and D shows that the amount of cell-surface mGluR1α slightly but significantly decreased when COS-7 cells were cotransfected with the intrinsic ligand-deficient Tamalin (Tamalin Δ8), as compared with the amount found with the full-length form (lanes 1 and 2). Furthermore, Figure 1E reveals that S-SCAM was co-immunoprecipitated with Flag-tagged (i) and non-tagged (ii) mGluR1α in the presence but not absence of myc–Tamalin using anti-Flag or anti-myc antibodies, suggesting that Tamalin forms a protein complex with mGluR1α and S-SCAM. These data predicted that the mGluR surface expression depends on the interaction of the intrinsic ligand with S-SCAM, and we thus transfected COS-7 cells with S-SCAM. Coexpression of S-SCAM resulted in an increase in the surface expression of mGluR1α in a dose-dependent manner (Figure 1C, lanes 1, 3, and 4). However, this expression was reduced when the cells were cotransfected with the C-terminal-truncated form of Tamalin, instead of the full-length form of Tamalin (Figure 1C, lanes 3 and 5). Thus, the cellular experiments indicated that mGluR is linked to S-SCAM via the C-terminal intrinsic ligand of Tamalin.

As the Tamalin C-terminus also possesses the ability to bind its own PDZ domain, we next expected that this moiety could also negatively regulate the access of mGluR C-terminus. To test this prediction, we performed yeast two-hybrid assays by monitoring the β-gal reporter activities induced by the interactions between the DNA binding domain (BD)-fused mGluR5 C-terminal nine-residue peptide and the activation domain (AD)-fused intact or intrinsic ligand-deficient forms of Tamalin (Figure 2A). The cells expressing AD-Tamalin Δ8 exhibited no growth; so we alternatively expressed the N-terminal 210 aa of Tamalin, Tamalin1–210. Figure 2B reveals that the interaction of the BD-mGluR5 C-terminus with AD-Tamalin is markedly weaker than that with the AD-Tamalin1–210. This result indicates that intrinsic ligand binding has an inhibitory effect on Tamalin/mGluR interaction.

To address the question of whether the inhibition occurs in an intra- or intermolecular manner, we assessed the dimerization efficiencies between the BD- and AD-fused intact or intrinsic ligand-deficient forms. To detect intrinsic ligand binding, we expressed high levels of the Tamalin mutant, which lacks the unstructured AR region as shown by circular dichroism spectra (Supplementary Figure 1), and its derivatives. Figure 2C shows that BD-ΔAR interacted with AD-ΔAR. However, the affinities between BD-ΔARΔ8 and AD-ΔAR and between BD-ΔAR and AD-Tamalin1–210 were markedly lower than that between the BD- and AD-ΔARs. The interaction of BD-ΔARΔ8 with AD-Tamalin1–210 yielded no β-gal activity, indicating that the intrinsic ligand contributes to intermolecular associations. Moreover, we detected significantly reduced β-gal activities with the interaction between BD- and AD-ΔARs in the presence of the mGluR5 C-terminal nine-residue peptide (Figure 2D), indicating that the detachment of the intrinsic ligand by mGluR binding induces dissociation of the homomeric assembly of Tamalin. These results cannot completely rule out the possibility that Tamalin adopts the intramolecular autoinhibited conformation, which is often observed in other signaling proteins (Pufall and Graves, 2002). However, our assays strongly suggest that, in the absence or at low concentration of mGluRs, Tamalin forms novel autoinhibited assemblies.

We investigated the extent of mGluR concentration required for its competitive binding to Tamalin by co-immunoprecipitation assay. We first confirmed that mGluR1α was specifically immunoprecipitated with myc-Tamalin using anti-myc antibody (Supplementary Figure 2A, lanes 1–4). Then, we titrated the transfection DNA of Flag-mGluR and performed immunoprecipitations for each input cell lysate. mGluR1α concentrations in each cell lysate were determined

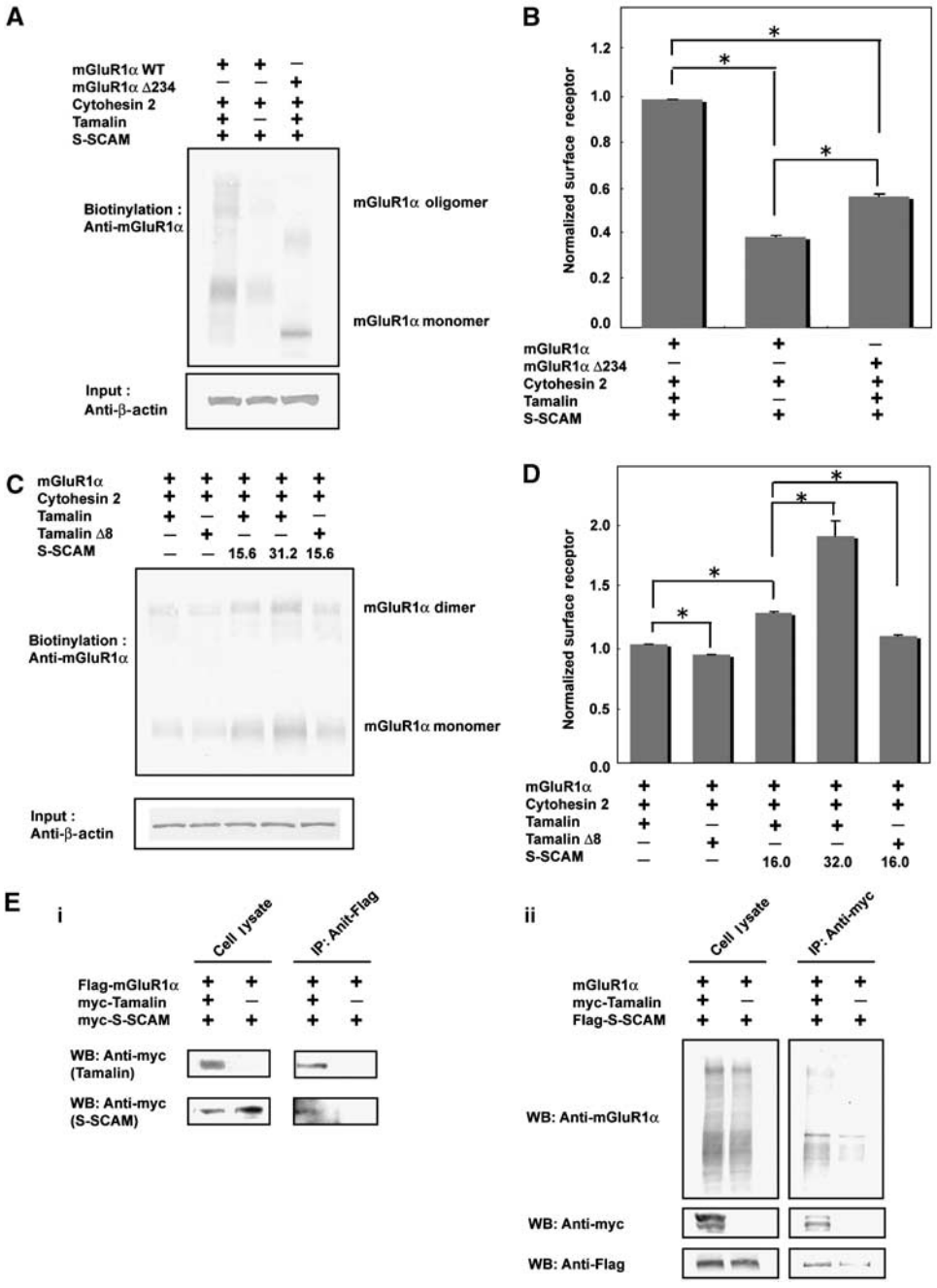

Figure 1 Increased cell-surface mGluR1α expression is dependent on the interaction of Tamalin with S-SCAM, via the C-terminal intrinsic ligand. (**A**) COS-7 cells were transfected with fixed amounts of plasmids containing EGFP-cytohesin (3.9 μg), myc-Tamalin (31.2 μg), and Flag-mGluR1α (3.9 μg), or its C-terminal 234-residue deletion mutant (3.9 μg). (**B**) Quantification of relative amounts of the cell-surface expression of mGluR1α and its deletion mutant. All values are expressed as mean ± s.d. Asterisks mark significant differences (Student's *t*-test; $^*P<0.05$). Experiments were repeated three times. (**C**) The cDNAs encoding mGluR1α, cytohesin, and Tamalin, or the C-terminal eight-residue-deficient variant of Tamalin were transfected into COS-7 cells with the plasmid encoding myc-S-SCAM (15.6 or 31.2 μg). Surface proteins were biotinylated, captured by avidin agarose, and analyzed by Western blots. For a reference, whole-cell lysates were subjected to β-actin immunoblots. (**D**) Quantification of relative amounts of cell-surface mGluR1α. Data are means ± s.d. Asterisks mark significant differences (Student's *t*-test; $^*P<0.05$). (**E**) Tamalin links mGluR1α to S-SCAM. COS-7 cells were triply transfected with Flag-mGluR1α, myc-Tamalin, and myc-S-SCAM (i) or non-tagged mGluR1α, myc-Tamalin, and Flag-S-SCAM (ii). Cell lysates were solubilized and immunoprecipitated with anti-Flag or anti-myc antibodies. Immunoprecipitates and cell lysates were blotted using anti-Flag, anti-myc, and anti-mGluR1α antibodies.

from the standard curve derived by using Flag-BAP control protein (Supplementary Figure 2B). The immunoprecipitated mGluR1α, which had been bound to Tamalin in each cell lysate, was blotted (Supplementary Figure 2A, lanes 5–10) and its amounts were also quantified. These values were plotted against mGluR1α concentrations in each cell lysate (Supplementary Figure 2C). This plot was fitted as the sigmoidal binding curve. These experiments showed that mGluR binding to Tamalin occurs at higher than an approximate concentration of 40 nM. Although the actual concentration of mGluR in the native tissues could not be determined, we envisaged that endogenous mGluR1α may

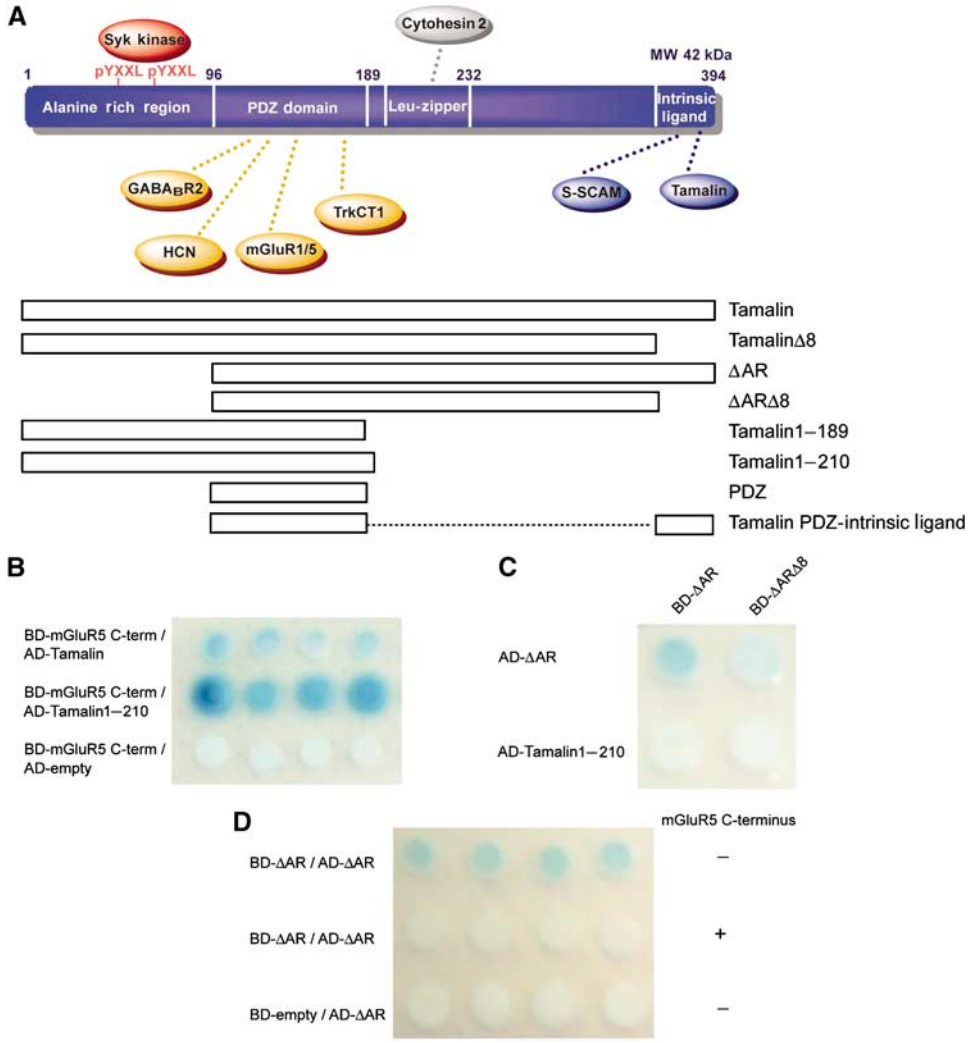

Figure 2 mGluR binding disrupts the autoinhibitory assemblies of Tamalin to liberate the Intrinsic ligand. (**A**) Schematic representation of the domain structure of Tamalin. Molecules identified as binding partners and the series of constructs used in this study are depicted. (**B, C**) Yeast two-hybrid assays of hetero- (B) and homotypic (C) interactions of Tamalin. The independent mating cultures were spotted and then assayed for β-gal activity. (**D**) Disruption of the autoinhibitory assembly of Tamalin by the binding of the mGluR5 C-terminal peptide. We utilized a pBridge vector (Clontech) instead of pAS2-1, in which the mGluR5 C-terminus was cloned or not into second multiple cloning site.

be sufficient to competitively bind to Tamalin and thereby release the intrinsic ligand from the PDZ domain.

Novel self-association mode of the Tamalin N-terminal region

To clarify the molecular details of Tamalin oligomerization, we tried to visualize the key protein–protein interactions at the atomic level. However, crystallization of the N-terminal region, Tamalin1–189, was unsuccessful. Thus, we performed limited proteolysis to analyze its domain architecture, and expressed the PDZ domain for biochemical characterization.

Gel filtration analyses revealed that the PDZ domain eluted mostly as the monomer (Figure 3A, peak b), but, at higher protein concentrations, the dimeric component (peak a) clearly increased (Figure 3Ai). We next conducted a dynamic light scattering (DLS) analysis, and found that the PDZ domain forms a dimer at a high concentration (300 μM) (Table I). To assess this monomer/dimer equilibrium, we performed an analytical ultracentrifugation analysis, and confirmed that the dissociation constant for dimerization is 222 μM (Figure 3B).

To clarify the molecular basis of the self-association of Tamalin, we determined the crystal structure of its PDZ domain in a ligand-free form at 1.8 Å resolution (Table II). The two molecules in the asymmetric unit are well superimposed, with an r.m.s.d. value of 0.59 Å between Cα atoms. The β2 and β3 strands from one protomer cross and pack against those from the other, forming a dimer interface burying a 713.5 $Å^2$ surface area per protomer (Figure 4A). This overall architecture differs from that of other PDZ dimers (Im *et al*, 2003a, b), where dimerization through the antiparallel N-terminal β1 strands has been commonly observed.

Hydrophobic residues are clustered at the center of the dimer interface, notably with the aromatic side chains of Tyr118 and Phe133 from each protomer (Figure 4B and Supplementary Figure 3A). One protomer also projects the side chains of Leu120 and Var131 to participate in these hydrophobic contacts with the counterpart of the dimer. In

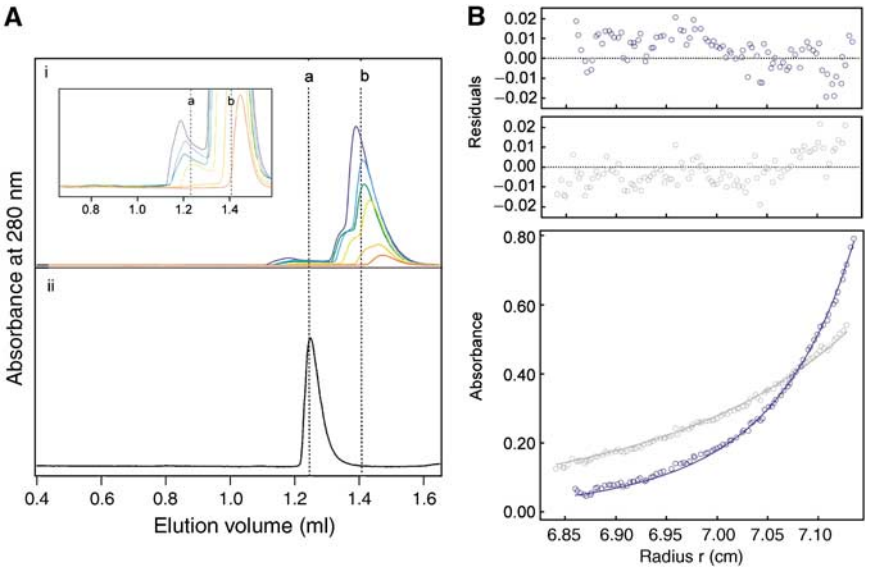

Figure 3 Characterization of the Dimeric N-terminal region of Tamalin. (**A**) Gel filtration analyses of the ligand-free and intrinsic ligand-bound PDZ domains. (i) The PDZ domain is in the monomer (peak b)/dimer (peak a) equilibrium. Increasing concentrations of protein were injected (red to blue), and the dimeric components clearly increased (inset). (ii) The Tamalin PDZ-Intrinsic ligand protein is detected as a dimer. (**B**) Analytical ultracentrifugation of the Tamalin PDZ domain. Shown are equilibrium sedimentation data obtained at 20 000 (gray circles) and 30 000 r.p.m. (blue circles) and the best-fit curves (solid line) for a monomer/dimer reversible equilibrium model.

Table I Dynamic light scattering analyses

	Mean	Radius (nm)	MW (kDa)	Baseline[a]	SOS error[b]
Tamalin PDZ domain	9	2.3	23	1.002	3.193
Tamalin PDZ-Intrinsic ligand wild-type	15	3.0	43	1.003	1.694
Tamalin PDZ-Intrinsic ligand Arg168Trp	7	2.7	33	1.005	1.859
Tamalin PDZ-Intrinsic ligand Arg168Ser	10	2.8	34	1.010	3.515

[a]Baseline represents the completeness and fit of the regression applied during the analysis.
[b]SOS error = sum of squares error, which is a measurement of the closeness of the fit between the experimental results and an autocorrelation function generated from the analysis results.

the vicinity of the core, the C-terminal portion is anchored to the other protomer by polar interactions. The bulky side chains of Gln116 and Arg136 protrude from the interface, thereby hitching one protomer to the other (Figure 4C). This dimeric structure keeps the two binding grooves open for interactions with binding partners. In particular, the TFGF loop, which binds the C-terminal carboxylate of the ligands, is located away from the interface (Figure 4A). Thus, hydrophobic interactions enable Tamalin to associate with its partners, while maintaining the PDZ dimerization.

Autoinhibitory association of the Tamalin PDZ domain with its intrinsic ligand: possible self-assembly modes of Tamalin

To address how Tamalin discriminates between the intrinsic and extrinsic targets (Supplementary Figure 3B), we examined their binding abilities by surface plasmon resonance (SPR) analyses. All of the curves were fitted to single site but not double site binding. The binding of the Tamalin C-terminus to the PDZ domain yielded a K_d value of 631 μM (Figure 5A and B, and Table III), which shows that this affinity is relatively low, whereas the binding of the mGluRs C-termini yielded K_d values of 135 and 85.3 μM, respectively. The lower affinity of the intrinsic ligand seems to be favorable for the extrinsic ligands to compete with and to replace the intrinsic ligand in the binding groove.

We tried to elucidate how Tamalin recognizes its own C-terminal ligand. To overcome the difficulties in crystallization with low-affinity ligand, we used a crystallization strategy, in which the intrinsic ligand was fused to the C-terminus of the PDZ domain, as used for the structural determination of other scaffold proteins (Feng *et al*, 2004) (Figure 2A). The crystal structure was consequently determined at 2.85 Å resolution (Table II).

The Tamalin PDZ-Intrinsic ligand protein exhibited a unique tetrameric structure, comprising a dimer of PDZ dimers (Figure 5C). This assembly is consistent with the results of the DLS analysis (Table I). In addition, the protomer orientation is not restrained by the artificial ligand fusion, but appears to reflect the native geometry, because the segments between the intrinsic ligand and the PDZ domain are poorly ordered. This notion is further supported by the fact that both dimers superimpose well onto the ligand-free PDZ dimer, with Cα r.m.s.d.s of 2.35 and 2.44 Å. Thus, these lines of evidence convinced us that the PDZ domains and the intrinsic ligands of the tetrameric configuration in the crystal represent behaviors in full-length Tamalin under biological conditions.

Table II Data collection and refinement statistics

Data collection and phasing	Ligand-free form	Tamalin PDZ-Intrinsic ligand (SeMet)			Tamalin PDZ-mGluR5 C-terminal tail complex
Space group	*C*2	$P2_12_12_1$	$P2_12_12_1$	$P2_12_12_1$	*I*422
Unit cell dimensions (*Å*)					
a	111.28	48.56	48.56	48.56	75.61
b	30.03	114.07	114.07	114.07	75.61
c	80.11	125.74	125.74	125.74	80.19
β (deg)	132.33	90.00	90.00	90.00	90.00
Wavelength (Å)	1.00000	0.97910	0.97940	0.99000	1.00000
Resolution (Å)	50.0–1.80	50.0–2.85	50.0–2.85	50.0–2.85	50.0–2.10
No. of reflections	66 815	319 183	287 716	288 553	238 912
Completeness (%)	99.3 (97.1)[a]	98.5 (88.5)[a]	97.0 (78.8)[a]	97.2 (79.6)[a]	99.6 (99.6)[a]
I/σ (I)	7.2	6.0	5.9	5.9	22.2
Redundancy	3.6	6.9	6.9	6.9	7.4
R_{merge} (%)[b]	9.1 (27.6)[a]	10.6 (38.2)[a]	10.8 (42.9)[a]	10.8 (39.6)[a]	3.7 (52.1)[a]
Figure of merit[c] (45.3–3.0 Å) (centric/acentric)				0.56/0.68	
Refinement					
Resolution range (Å)	50.0–1.80			50.0–2.85	50.0–2.40
R_{cryst}/R_{free}[d]	23.5/26.7			26.9/29.1	25.9/27.3
Number of atoms (protein/water)	1369/107			2698/43	646/10
Average *B*-factor (protein/solvent) (Å)	12.9/19.3			39.2/35.2	49.9/51.8
Ramachandran (favored, allowed, generous, and disallowed) (%)[e]	95.9, 3.4, 0.7, 0.0			82.3, 16.7, 1.0, 0.0	90.5, 6.8, 2.7, 0.0

[a]Values in parentheses indicate statistics for the last shell.
[b]$R_{merge} = (\sum|I_I\langle I_I\rangle|)/\sum_I|I_I|$, where $\langle I_I\rangle$ is the mean I_I over symmetry-equivalent reflections.
[c]Figure of merit $= \langle \sum P(\alpha)\exp(I\alpha)/\sum P(\alpha)\rangle$, where $P(\alpha)$ is the phase probability at angle α.
[d]R_{free} was calculated using 5% of total reflections, which were chosen randomly and omitted from the refinement.
[e]Calculated by the program PROCHECK (Laskowski *et al*, 1993).

This assembly preserves the dimer interface interaction, as shown in the ligand-free form (Figure 4), and creates a dimer–dimer interface, with a buried surface area of 2601.0 $Å^2$ (Figure 5C). This interface involves polar interactions between two PDZ dimers. In particular, the α2 helices of each dimer mutually form salt bridges between Arg168 and Asp172, which appear to stabilize the dimer–dimer association (Figure 5D). Moreover, the intrinsic ligand binds to the adjacent protomer across both the dimer and dimer–dimer interfaces.

The intrinsic ligand binding affects the oligomeric states of Tamalin. The biochemical analyses suggest that the Tamalin PDZ-Intrinsic ligand protein acts as a dimeric species, as shown by the gel filtration analysis, but the tetrameric state is predominant at a higher concentration, such as in the DLS and crystallized conditions (>300 μM) (Figure 3Aii and Table I). These results are in contrast with the results of the above biochemical analyses of the ligand-free PDZ domain, in which Tamalin was suggested to be in a dimer/monomer equilibrium (Figures 3 and 4). Thus, Tamalin changes its oligomeric form, depending on its concentration and intrinsic ligand binding: intrinsic ligand binding induces Tamalin to adopt the higher-order oligomeric states, tetramer and dimer, whereas upon detachment of the ligand, Tamalin exists in a lower-order oligomeric equilibrium between the dimer and monomer.

To confirm the functional importance of the oligomeric assembly of Tamalin, we constructed two types of Tamalin PDZ-Intrinsic ligand protein mutants: Arg168 was replaced by Trp with a bulky side chain that might cause steric hindrance between protomers, and a smaller residue Ser that might eliminate the specific interactions. The DLS analyses showed that in contrast with a 43 kDa molecular mass of the Tamalin PDZ-Intrinsic ligand protein, those of the Arg168Trp and Arg168Ser mutants were estimated at 33 and 34 kDa, respectively (Table I). These data indicated that a tetramer/dimer equilibrium shifted toward a dimeric or trimeric component, leading to the disappearance of tetrameric species. We also replaced Arg168 of the full-length Tamalin with Trp and Ser and cotransfected them with mGluR1α into COS-7 cells. Cotransfection of these mutants significantly increased the cell-surface expression of mGluR1α in the presence of S-SCAM, as compared with cotransfection with wild-type Tamalin (Figure 5E). Thus, these results support the biological importance of the oligomeric autoinhibitory associations of Tamalin.

Autoinhibitory association of the Tamalin PDZ domain with its intrinsic ligand: two distinct ligand recognition modes

The most important feature in association with the intrinsic ligand is that the ligand occludes the adjacent groove in two distinct modes: conventional and unconventional (Figure 5C). In the intrinsic ligand-bound PDZ dimer detected only biochemically, the ligands are likely to bind to the adjacent protomers in only the conventional manner, as revealed by the mGluR C-terminus complex structure (see below). On the other hand, in the tetrameric assembly, the intrinsic ligands of two protomers of one dimeric unit interact with the groove in the counterpart of the dimer by the

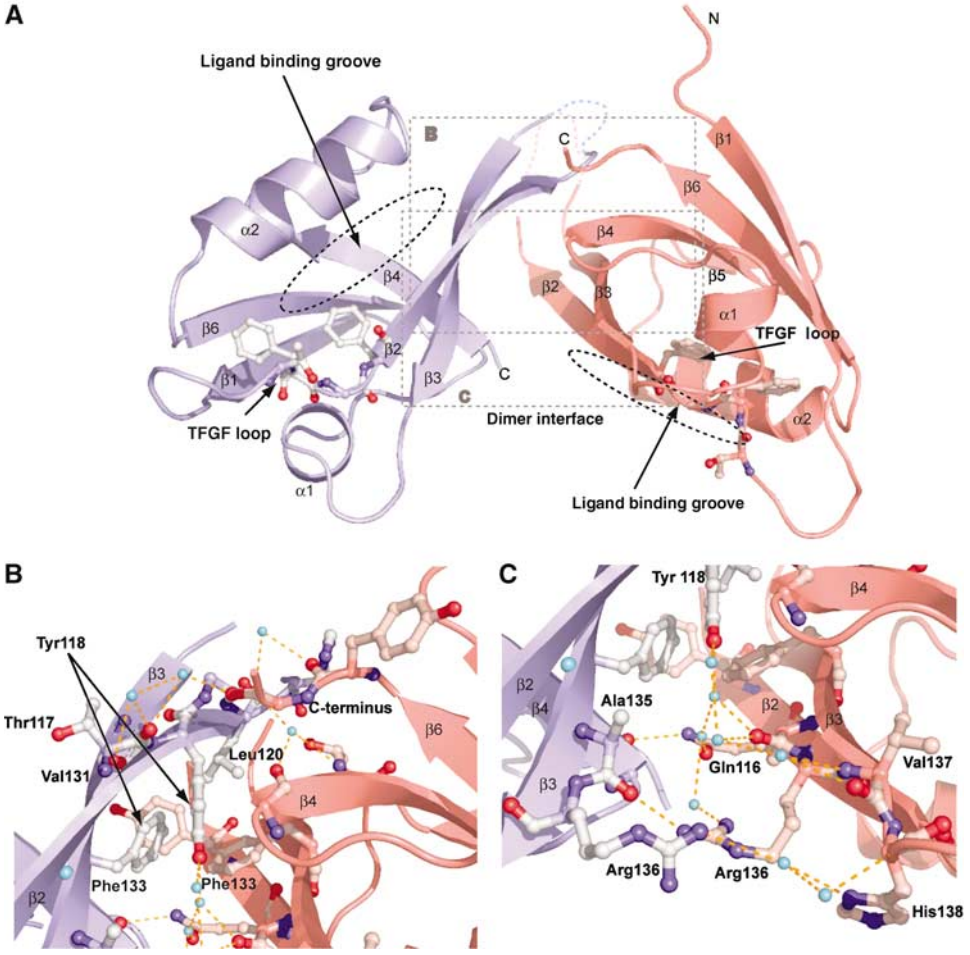

Figure 4 Novel dimeric architecture of Tamalin PDZ domain in the intrinsic ligand-unbound state. (**A**) Dimeric structure of the PDZ domain. Protomers A and B are colored light blue and magenta, respectively. The blue and magenta dotted lines represent the disordered β2–β3 loops. The TFGF loop is shown as a ball-and-stick model. (**B, C**) Close-up views of the upper (B) and lower (C) regions in the dimer interface, as indicated in (A). Dashed lines indicate hydrogen bonds and ion pair interactions.

Table III Summary of the dissociation constants for the Tamalin PDZ binding peptides

Protein	Sequence	Wild-type K_d (μM)	Glu114Lys K_d (μM)
mGluR1 (467.4 RU)[a]	LRDYKQSSSTL	135	162
mGluR5 (449.8 RU)[a]	IRDYTQSSSSL	85.3	160
Ser-1Ala/Ser-3Ala (426.8 RU)[a]	IRDYTQSASAL	181	ND
Intrinsic Ligand (540.8 RU)[a]	NRSLEEEESQL	631	74.6

[a]Values in parentheses indicate the amount of immobilized peptides as response units. ND, not determined.

conventional mode, and with that of a protomer in the other dimer by the unconventional mode.

In the conventional mode, the ligand backbone adopts a β-strand, and the consensus residues, Leu0 and Ser-2, form canonical interactions with the binding grooves (Figure 6A and Supplementary Figure 4A). On the other hand, the non-consensus side chains form no favorable interactions that augment the binding affinity, except for Gln-1, which contacts His138. Besides these few interactions, the side chain of Glu-3 points away from Glu114, which is a key residue in mGluR5 ligand binding, as described below. Considering the results of the biochemical characterization of intrinsic ligand binding (see below), this situation is attributed to the electrostatic repulsion between the carboxyl groups of Glu-3 and Glu114. Thus, the smaller number of favorable interactions and the electrostatic effect selectively lower the binding activity of the intrinsic ligand.

In the unconventional mode, the intrinsic ligand is perpendicularly oriented toward the groove in the other dimer, in contrast to other PDZ ligands that adopt a β-strand antiparallel to the PDZ grooves (Figure 6B and Supplementary Figure 4B). This orientation resembles the autoinhibited conformation of the X11α/Mint1 PDZ domain reported recently (Long *et al*, 2005) (Figure 6C), except for some significant differences. The characteristic feature of the X11α/Mint1 structure is the narrowness of the groove, which hampers the formation of an antiparallel β-strand by its ligand. In contrast, the superimposition of the Tamalin structures indicated no

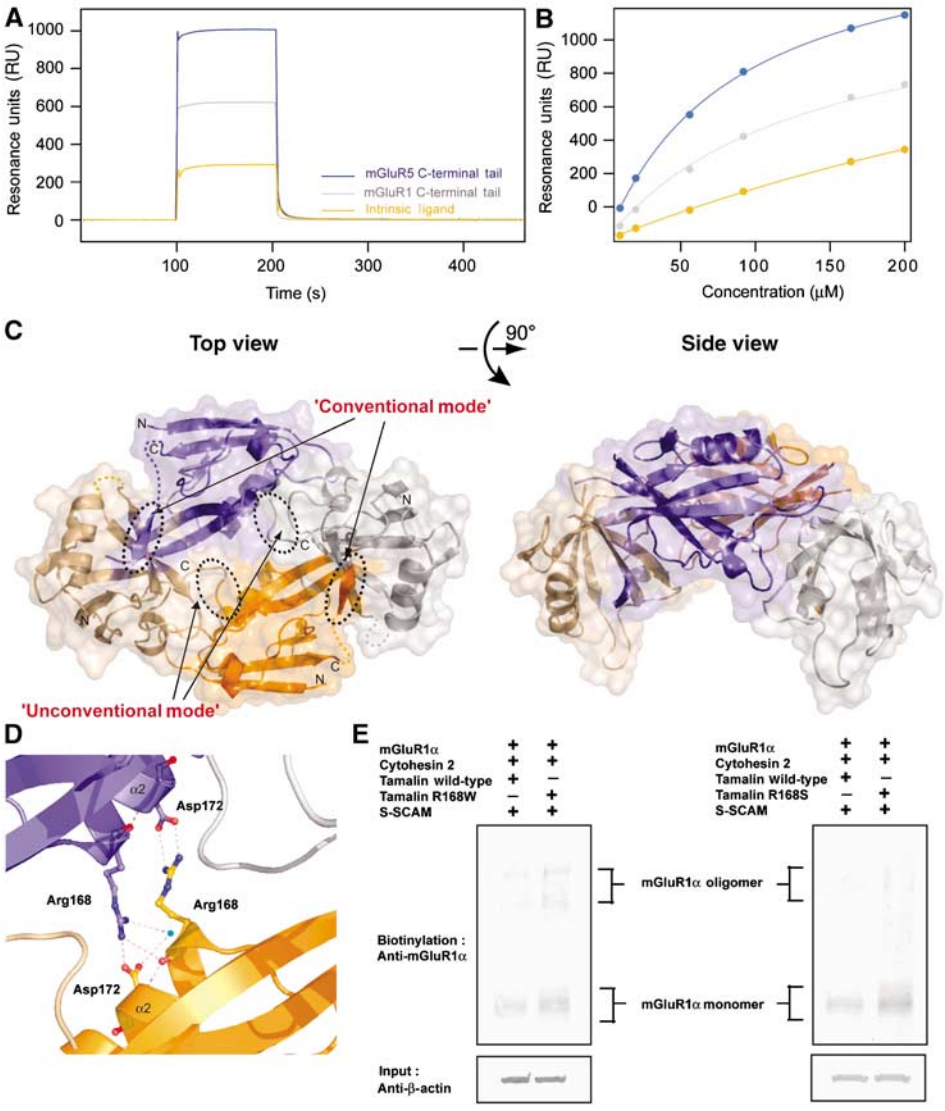

Figure 5 The hydrophobic dimerization interface and two types of PDZ/ligand interactions form an integral part of the autoinhibited assembly. (**A**) Loose binding of the Tamalin C-terminus to its own PDZ domain. The binding abilities of each C-terminus were measured using SPR analyses. The sensorgrams from a representative concentration, 92 μM, are shown. (**B**) Steady-state equilibrium responses from the sensorgrams were plotted against the injected PDZ concentrations. (**C**) Tetrameric assembly of the Tamalin PDZ-Intrinsic ligand protein. The N- and C-termini of the PDZ domains are described. The assembly involves two hydrophobic interaction-mediated PDZ dimers (blue and magenta, or gray and orange). The binding grooves are occluded by the intrinsic ligands in the conventional and unconventional manners. (**D**) Essential salt bridges between the two PDZ dimers. The orientation of the PDZ dimers is identical to that in Figure 4A. (**E**) Arg168Trp or Arg168Ser mutation of Tamalin increases the cell-surface expression of mGluR1α. COS-7 cells were transfected with plasmids encoding mGluR1α, EGFP-cytohesin 2, myc-S-SCAM, and myc-Tamalin, or myc-Tamalin mutants, as indicated.

drastic structural deference between the unconventional and conventional modes, as revealed from the r.m.s.d. value of 0.77 Å. Thus, instead of the specific conformational constraint of the groove in X11α/Mint 1, the Tamalin PDZ domain harbors sufficient capacity for ligand interactions in both binding modes.

The C-terminal end of the intrinsic ligand inserts itself into a hydrophobic pocket, formed by Ile174 and the TFGF loop, and this structural feature closely resembles the canonical interaction observed in other PDZ/ligand interactions (Figure 6B and D). Each main chain of Ser-2 and Glu-3 interacts with His167 through two water molecules and with Lys175. However, these interactions are observed in either of the two unconventional binding sites. The penultimate residue, Gln-1, is fixed to a perpendicular orientation by its specific side-chain interactions. Structural comparisons of the penultimate residue also revealed significant differences in the interaction mode between the X11α/Mint1 and Tamalin PDZ domains. In the former, the hydrophobic Tyr-1 fits snugly into a hydrophobic pocket formed by Ile666, Val670, and Met689 (Figure 6C). In contrast, the Tamalin PDZ domain has the hydrophilic Glu114 and His138 residues in place of the hydrophobic Ile666 and Met689 residues, respectively (Figure 6D). As a result, the side chain of Gln-1 can form robust polar interactions with the side chains of Glu114 and His138. Thus, the groove in the Tamalin PDZ domain is feasible to flexibly adjust to ligand binding both in conventional and unconventional modes. Despite such specific interactions by the C-terminal two residues, this mode lacks the backbone interactions required to form the β-strand

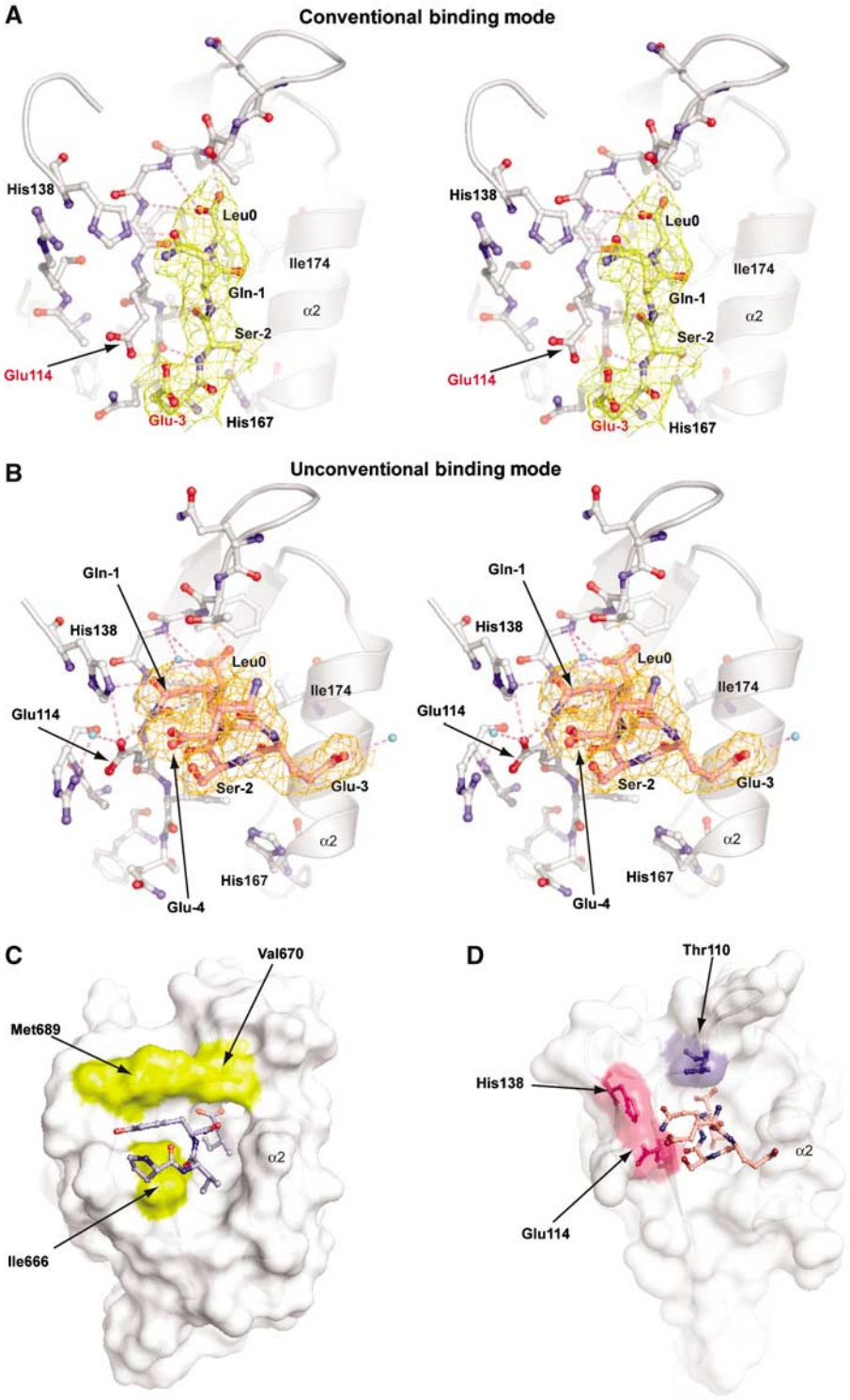

Figure 6 Canonical and noncanonical autoinhibitory PDZ/intrinsic ligand interaction modes. (**A, B**) Conventional (A) and unconventional (B) modes are illustrated as stereo diagrams. Residues involved in the electrostatic repulsion are labeled with red letters in the conventional mode. The $2F_o$–F_c electron density maps are displayed for the intrinsic ligands. (**C, D**) Comparison of the perpendicularly oriented modes of the Mint1/X11α (C) and Tamalin PDZ domains (D), shown by surface representation. Key hydrophobic residues that interact with the penultimate residue are colored yellow in the Mint1/X11α PDZ domain. Residues forming hydrophilic interactions with the penultimate residue of the intrinsic ligand are colored magenta, and those not forming interactions are shown in purple in the Tamalin PDZ domains.

element. Although we could not confirm the affinity difference between the two binding modes by SPR analyses, the much less interactions in the unconventional mode also appear to be responsible for the lower affinity of the intrinsic ligand.

Structural determinant for binding of the mGluR C-terminal tail to the Tamalin PDZ domain

To elucidate how the PDZ binding motif of mGluR relieves the autoinhibition, we determined the structure of the Tamalin PDZ domain-mGluR5 C-terminus complex at 2.4 Å resolution

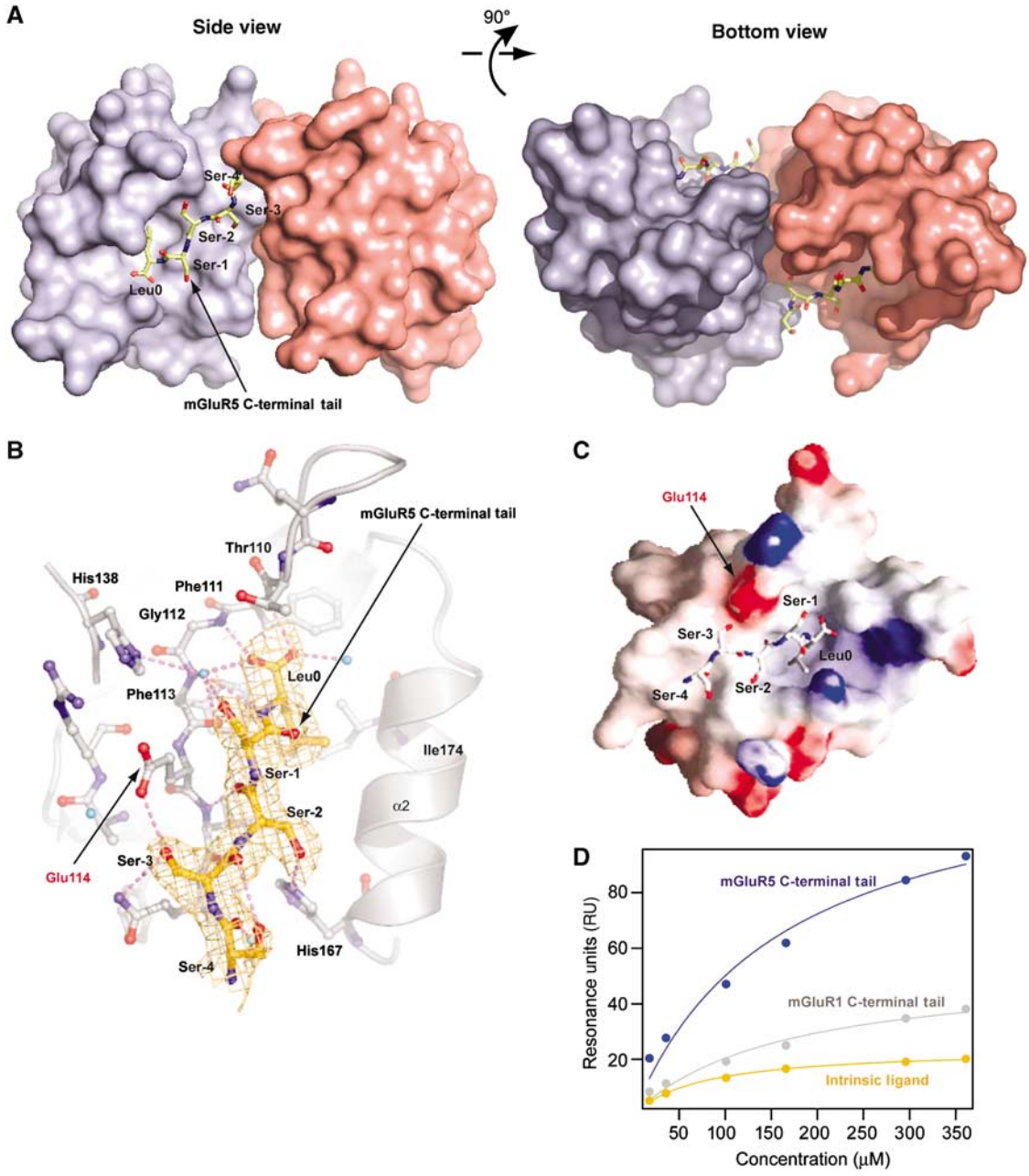

Figure 7 Role of the electrostatic effect in the mGluR C-terminus/Tamalin PDZ domain interaction. Overall structure (**A**) and a close-up view (**B**) of the Tamalin PDZ-mGluR5 C-terminus complex. (A) The orientation of the PDZ dimers in the side view is identical to that in Figure 4A. (**C**) Electrostatic surface potential from approximately $-10k_BT^{-1}$ (red) to $+10k_BT^{-1}$ (blue). The negative charge of Glu114, which may contribute to the electrostatic interaction with mGluR5, is indicated by an arrow. (**D**) SPR analyses of the binding of the mGluRs and Tamalin C-termini to the Glu114Lys PDZ mutant.

(Table II), using the same strategy as for the Tamalin PDZ-Intrinsic ligand protein. The asymmetric unit contains one molecule, which forms a dimer with a symmetry-related protomer. This dimeric architecture superimposes well on that of the ligand-free form, including the hydrophobic dimerization interface. A cytoplasmic tail of a dimeric mGluR binds to each Tamalin binding pocket that is far from its own dimer interface, and thus the complex of Tamalin with mGluR is formed with a 2:2 stoichiometric ratio (Figure 7A). This complex formation, involving the two contiguous cytoplasmic domains of a dimeric mGluR, may reinforce rather a weak hydrophobic interaction between two Tamalin PDZ domains.

In contrast to the intrinsic ligand, the mGluR5 C-terminus adopts only the conventional mode (Figure 7B). The consensus residues also form canonical interactions with the binding grooves. The side chain of Ser-1, a non-consensus residue, forms water-mediated hydrogen bonds with the side chain of His138 and the main chain of Phe113 in the binding groove. Furthermore, the side chain of Ser-3 interacts with the γ-carboxyl group of Glu114 possibly by a hydrogen bond (Figure 7C). These structural observations allowed us to assume that the hydrogen bonds of Ser-1 and Ser-3 contribute to the higher affinity of the mGluR5 C-terminus relative to that of the intrinsic ligand.

To examine this possibility, we performed a binding assay, revealing that the Ser-1Ala/Ser-3Ala double mutation of mGluR5 C-terminus increases the K_d, as described in Table III. Meanwhile, this result does not appear to explain fully the affinity difference between the mGluR5 C-terminus and the intrinsic ligand. The crystal structure (Figure 6A) implies that the electrostatic repulsion selectively reduces the affinity of the intrinsic ligand. Consistent with this, the Glu114Lys mutation increased the K_d of the mGluR5 C-terminus and reduced that of the intrinsic ligand (Figure 7D and Table III). Thus, the electrostatic property of Glu114 weakens and strengthens the intrinsic and extrinsic ligand affinities, respectively, and thereby substantially confers specificity on the PDZ/ligand interaction.

Discussion

Novel structural and functional features of the PDZ domain

Here, we provided the atomic view of the key interactions between mGluR and its scaffold protein Tamalin. These interactions include novel oligomeric and ligand recognition modes that could play pivotal roles in regulating mGluR trafficking process.

The Tamalin PDZ domain constitutes the hydrophobic core in the dimer interface, which functions in stabilizing its oligomeric assembly. The interface might be unique to Tamalin, because the key hydrophobic residues, Tyr118 and Leu120, are not conserved in other PDZ dimers (Supplementary Figure 3A). In fact, this dimeric architecture is quite distinct from that of other PDZ homodimers, suggesting that the dimeric configuration of the PDZ domain is unexpectedly variable. The particular dimeric configuration may be arranged to efficiently accommodate the conformation of each binding partner, thereby making the PDZ-containing scaffolds specifically adapted for protein assembly.

The restriction of the scaffolding activity is directed by two modes of interprotomer interaction. It should be noted that both conventional and unconventional modes display few interactions with the binding grooves. Therefore, mGluR could specifically compete off the weak intrinsic ligand binding. Thus, the autoinhibitory activities appear to stabilize the oligomeric assembly and to halt the scaffolding action until Tamalin encounters the extrinsic ligands. This is the first evidence for the dual role of the intrinsic ligand.

Several authors have mentioned diversity in the ligand recognition activities of the synaptic PDZ proteins (Hung and Sheng, 2002; Penkert *et al*, 2004). PDZ domains can recognize not only the C-terminal motif but also the non-C-terminal 'internal' sequences (Hillier *et al*, 1999). The perpendicular orientation was observed in the X11α/Mint protein, and was ascribed to its unique conformational constraints in the binding groove (Long *et al*, 2005). Here, we have demonstrated that Tamalin can adopt perpendicular orientations, which do not require specific conformational constraints, but can be formed by hydrophilic interactions through the penultimate residue. These observations led us to infer that this orientation is more common than previously thought, especially in the case of the autoinhibitory PDZ proteins, in which the ligand interactions should be weak and easily disrupted by other targets. Collectively, the PDZ proteins are suggested to recognize the ligand backbone in at least three distinct manners: the conventional mode, the non-terminal sequence recognition mode, and the perpendicularly oriented mode.

Implications for mGluR trafficking regulation by Tamalin

Although associations with various scaffold proteins are known to be essential for GPCR trafficking (Lefkowitz and Shenoy, 2005), the molecular mechanisms have remained elusive. In particular, the determinant of dendritic localization in mGluR remained unclear. Tamalin has been implicated in mGluR trafficking between cell bodies and neurites (Kitano *et al*, 2002). During preparation of the manuscript, however, Das and Banker (2006) showed that deletion of the entire C-terminus of mGluR1α only modestly affects its trafficking to dendrites in cultured hippocampal neurons. They suggested that mGluR1α contains redundant targeting signals and, in the absence of the C-terminus, other regions of the receptor are capable of maintaining its dendritic targeting to a large degree. On the other hand, Tamalin seems to be an attractive candidate to study the class III/C GPCR organization, as it has the ability to associate with the cytoplasmic sides of not only mGluRs but also another metabotropic receptor, $GABA_B$ receptor. Indeed, the current study has presented structural evidence for a direct mGluR5/Tamalin interaction. Therefore, we discuss the scaffolding mechanism of Tamalin possibly regulating mGluR organization and trafficking.

After translation, Tamalin protomers would encounter each other, merge, and then form the autoinhibitory conformation (Figure 8). The increase in the physiological concentration likely shifts the oligomeric equilibrium toward the tetramer. In the absence or probably at low concentrations of mGluRs, these conformations lock the intrinsic ligand in the inactive state, to restrict mGluR binding and to prevent the subcellular trafficking of Tamalin alone. The autoinhibited assemblies may serve to provide a reserve of rapidly available Tamalin. Yeast three-hybrid assays revealed that cytohesin 2 could constitutively bind to the inhibited and its released conformations (data not shown).

In these processes, one of the key questions is why Tamalin adopts these oligomeric forms. Our previous biochemical and X-ray structural analyses revealed that the extracellular region of mGluR1 exists as a dimer, formed by a hydrophobic interface and a disulfide bridge (Kunishima *et al*, 2000; Tsuji *et al*, 2000). In addition, recent biochemical studies, including FRET analyses, have provided ample data that many GPCRs also function as obligate dimers (Bulenger *et al*, 2005). However, it is unclear how the mGluR dimer is organized within subcellular compartments. Tamalin may contribute to the facilitation of mGluR dimerization upon its trafficking because, once the concentration of mGluR reaches a level required for the replacement of the intrinsic ligand, an oligomeric Tamalin can recruit multiple mGluR protomers into close proximity on the binding grooves. The assemblies of scaffold proteins and the obligate dimerization of its binding partner were well studied in apoptotic signaling pathways, in which the multimeric adaptor proteins provide multiple binding sites for the monomeric caspases, thereby facilitating their dimerization and inducing their autoproteolytic activation (Shi, 2004). Likewise, the close proximity may increase the likelihood of interactions between mGluR

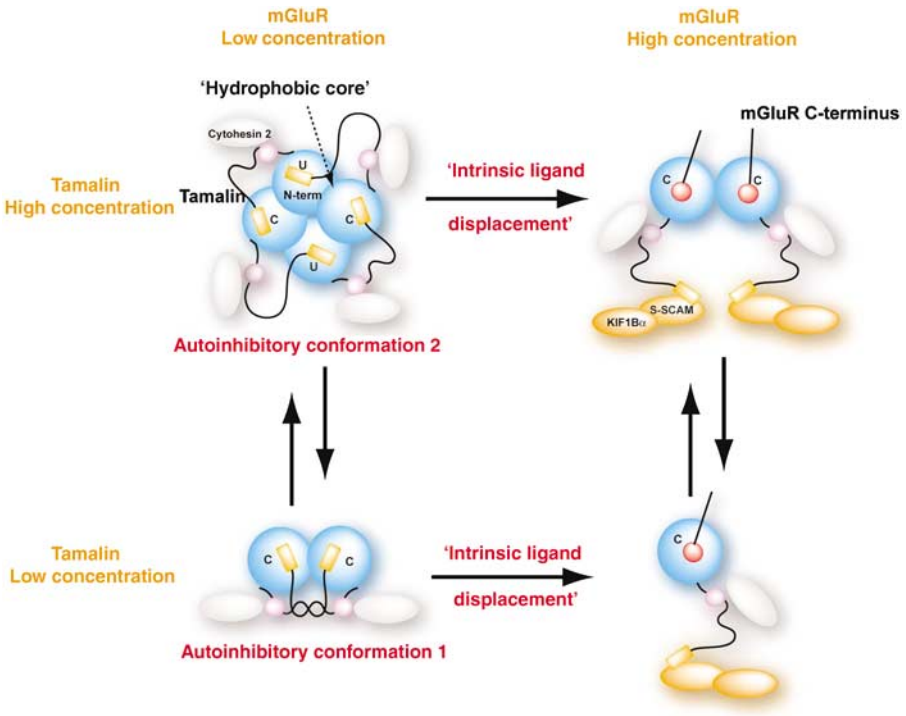

Figure 8 Mechanistic model for mGluR trafficking by Tamalin. Unconventional and conventional modes are indicated (U and C). The Leu-zipper-like region is colored purple. N-term denotes the N-terminal half of Tamalin, which includes the AR region and the PDZ domain. The Tamalin C-terminal intrinsic ligand is shown in yellow square.

protomers on the binding platform, thereby facilitating their oligomerization.

At a high concentration of mGluR, which disrupts the autoinhibited assemblies of Tamalin (Figures 2D and 8, and Supplementary Figure 2), a dimeric Tamalin should dissociate into monomers, owing to the loss of their intrinsic ligand interactions. However, Tamalin, at a high concentration, could dimerize under mGluR dimers, as revealed by our crystallographic analyses (Figure 7A). Tamalin might behave like beads on a string under two contiguous C-termini from two protomers of a dimeric mGluR or from two adjacent dimeric mGluRs, which may stabilize PDZ dimerization and contribute to amplifying the assembly of signaling molecules. In these conformations, an intrinsic ligand becomes exposed for S-SCAM, like those of other cargo receptor/scaffold protein/motor protein macrocomplexes (Kim and Sheng, 2004; Kneussel, 2005). We also provided evidence supporting the proposal that the association of the Tamalin C-terminus with S-SCAM facilitates mGluR cell-surface expression (Figure 1). Thus, Tamalin may change its assembly state from the autoinhibited to released forms, depending on the intracellular mGluR concentration, thereby regulating its cell-surface expression.

In this study, we have clarified a novel regulatory mechanism of the Tamalin autoinhibitory PDZ domain, which may control mGluR trafficking. Interestingly, recent reports have also described an autoinhibition mechanism for kinesin motor proteins, where cargo binding to kinesin de-represses a tail-mediated motor domain inhibition. This mechanism couples cargo binding and motor regulation (Adio *et al*, 2006). Therefore, autoregulation might be a fundamental process for protein trafficking. Especially, it is tempting to speculate that Tamalin also mediates the membrane targeting of other GPCRs, through its autoregulatory mechanism. Future studies are required to define the molecular mechanisms for GPCRs trafficking and to determine how Tamalin contributes to these dynamic processes.

Materials and methods

Cell-surface biotinylation assay

For the estimation of cell-surface expression level of mGluR1α and its mutant, cell-surface protein isolation kit (Pierce) was used according to the manufacturer's protocol, with some modifications. The plasmids for pCMV-Tag2B and -Tag3B (Stratagene), pEGFP C2 (Clontech) and pcDNA3.1 (Invitrogen) were utilized for assays. Subconfluent COS-7 cells were transfected with the Lipofectamine 2000 (Invitrogen) in a 75-cm^2 dish in serum-free medium for 4 h and then in medium containing serum for 20 h. For surface protein crosslinking, cells were incubated with 0.25 mg/ml of Sulfo-NHS-LC-S-S-Biotin for 30 min at 4°C. The crosslinking was terminated by the addition of quenching buffer and the cells were homogenized by sonication. Biotinylated proteins were captured using 200 μl of a NeutrAvidin agarose suspension for 1 h at 4°C, followed by elution in SDS sample buffer containing 50 mM DTT. Samples were analyzed by Western blotting. ImageJ software (National Institutes of Health) was used to quantify the band intensities. The amount of biotinylated mGluR1α in each sample was normalized by the amount of actin in cell lysates.

Immunoprecipitation assay

Subconfluent COS-7 cells were transfected in a 100-mm dish. Transfected COS-7 cells were lysed in RIPA buffer. Immunoprecipitation of myc-Tamalin and Flag-mGluR1α was carried out with anti-myc antibody-conjugated beads (Sigma) and anti-Flag M2 agarose beads (Sigma), respectively. Cell lysates or immunoprecipitates were subjected to Western blot analysis with anti-myc (Sigma), anti-Flag (Sigma), or anti-mGluR1α (BD Biosciences) antibodies.

Yeast two-hybrid assay

Yeast strains, Y187 and Y190, were transformed with the AD-fused protein expression vector, pACT2 (Clontech), and the BD-fused

protein expression vector, pAS2-1 (Clontech), respectively, by the lithium acetate method. The transformants were mated on YPD plates and diploids were repeatedly streaked and then spotted onto SD plates lacking Leu and Trp. For β-gal assays, each plate was incubated with 5 ml chloroform for 5 min and then with a 1.0 mg/ml X-gal solution containing 0.1% agar.

In vitro protein expression

The gene encoding Tamalin1–189 protein was cloned into the pTYB11 vector and protein was expressed and purified using the IMPACT system (New England Biolabs). The gene encoding the rat Tamalin PDZ domain was cloned into the vector pGEX-4T1 (Amersham Pharmacia). Fusion proteins were constructed by connecting the DNA fragments encoding the last five residues of the rat mGluR5 and Tamalin to the C-terminus of the PDZ domain. These proteins were expressed and purified using glutathione–Sepharose resin (Amersham Pharmacia). The GST tag of each protein was removed by thrombin digestion (1 U/ml). Tamalin1–189 protein, the PDZ domain, and Tamalin PDZ-Intrinsic ligand protein were purified on a Q-Sepharose column, followed by fractionation on a Superdex 75 gel filtration column equilibrated with the crystallization buffer. The Tamalin PDZ-mGluR5 C-terminus complex was purified on an SP–Sepharose column.

To prepare the SeMet derivative of the Tamalin PDZ-Intrinsic ligand protein, the constructed vector was transformed into the methionine auxotrophic strain *Escherichia coli* BL21 (DE3) RIL-X (Stratagene). The SeMet derivative was expressed by IPTG induction in medium containing seleno-L-methionine at a final concentration of 25 mg/ml and was purified using the same procedure as for the native protein.

DLS and analytical ultracentrifugation

DLS was performed using a DynaPro-801 instrument (Protein Solutions Inc.). The buffer contained 10 mM HEPES, pH 7.4, 150 mM NaCl, and 3.7 mg/ml protein. Data were analyzed with the regulation algorithm Dynamics 5.25.

Analytical centrifugation was performed on a Beckman XL-A centrifuge at 4°C. Protein solutions were loaded at an initial concentration of 159 μM and were analyzed at rotor speeds of 20 000 and 30 000 r.p.m. When fitted as a single ideal species, the obtained data yielded highly systematic residual deviations. The fitting was improved using an equilibrium dimer model.

Surface plasmon resonance

SPR measurements were performed using a BIAcore2000 at 24°C. The synthetic, biotinylated undeca-peptides were immobilized on the SA biosensor chip. Equilibrium experiments were performed by injecting the PDZ domain and its mutant at a flow rate of 5 μl/min.

Gel filtration experiment

Aliquots (20 μl) were loaded on a Superdex 75 PC3.2/30 column attached to a SMART chromatographic system (Amersham Pharmacia) at a flow rate of 40 μl/min. The column was pre-equilibrated with a buffer containing 10 mM HEPES, pH 7.4, and 150 mM NaCl.

Crystallization, data collection, and model refinement

Proteins were crystallized by the hanging drop vapor diffusion method at 20°C. Crystallization drops were prepared by mixing 0.5 μl of a 3.2 mg/ml protein solution with 0.5 μl of reservoir solution. Monoclinic crystals of the PDZ domain were grown in 20% PEG 3350 and 0.2 M potassium fluoride, pH 7.2. Crystals were soaked for a few minutes in the reservoir solution supplemented with 30% ethylene glycol and flash frozen in an N_2 stream. The SeMet Tamalin PDZ-Intrinsic ligand protein and mGluR5 C-terminus complex were crystallized in reservoir solutions containing 0.1 M HEPES, pH 7.5, 0.8 M sodium dihydrogen phosphate, and 0.8 M potassium dihydrogen phosphate, and in 0.1 M tri-sodium citrate dihydrogen and 1.0 M ammonium dihydrogen phosphate, pH 5.6, respectively. Each crystal was cryoprotected in 25% (v/v) ethylene glycol and 25% glycerol (v/v) for 5 min, followed by flash freezing in an N_2 stream. Diffraction data were collected at the Photon Factory and the SPring-8, Japan. All data were processed using HKL2000 (Otwinowski and Minor, 1997).

The structure of the PDZ domain was solved by the molecular replacement method, using CNS (Brunger *et al*, 1998) and the hNHERF PDZ1 as a search model (Karthikeyan *et al*, 2001). The properly positioned molecule was refined with CNS and O (Jones *et al*, 1991). The MAD phasing for the Tamalin PDZ-Intrinsic ligand protein was performed using data from the SeMet derivative. The positions of the four selenium atoms were determined from an anomalous Patterson map, and then the phases were calculated using SHARP (de La Fortelle and Bricogne, 1997). The MAD phases were improved by density modification with DM (CCP4, 1994). During the refinement, two phosphate molecules were found near the segments preceding the unconventionally bound intrinsic ligands. The tetramer was observed in a solution without phosphates (Table I), implying that these ions would be bound to and stabilize the tetrameric structure within the crystals. The mGluR5 C-terminus complex structure was determined by the molecular replacement method, using the PDZ domain as a probe. After density modification of the initial model using SOLOMON, the model was further refined to convergence. The coordinates for the crystals of the ligand-free PDZ domain, Tamalin PDZ-Intrinsic ligand protein, and Tamalin PDZ-mGluR5 C-terminal tail complex have been deposited in the PDB codes, 2EGO, 2EGK, and 2EGN, respectively.

Supplementary data

Supplementary data are available at *The EMBO Journal* Online (http://www.embojournal.org).

Acknowledgements

We thank Dr Izuru Ohki for experimental advice and Dr Yoshikazu Suzuki for discussions and critical reading of the manuscript. This work was partly supported by a research grant endorsed by the New Energy and Industrial Technology Development Organization (NEDO).

References

Adio S, Reth J, Bathe F, Woehlke G (2006) Review: regulation mechanisms of Kinesin-1. *J Muscle Res Cell Motil* **27:** 153–160

Brunger AT, Adams PD, Clore GM, DeLano WL, Gros P, Grosse-Kunstleve RW, Jiang JS, Kuszewski J, Nilges M, Pannu NS, Read RJ, Rice LM, Simonson T, Warren GL (1998) Crystallography & NMR system: a new software suite for macromolecular structure determination. *Acta Crystallogr D* **54** (Part 5)**:** 905–921

Bulenger S, Marullo S, Bouvier M (2005) Emerging role of homo- and heterodimerization in G-protein-coupled receptor biosynthesis and maturation. *Trends Pharmacol Sci* **26:** 131–137

Collaborative Computational Project n.4 (1994) The CCP4 suite: programs for protein crystallography. *Acta Crystallogr D* **50:** 760–763

Das SS, Banker GA (2006) The role of protein interaction motifs in regulating the polarity and clustering of the metabotropic glutamate receptor mGluR1a. *J Neurosci* **26:** 8115–8125

de La Fortelle E, Bricogne G (1997) Maximum-likelihood heavy-atom parameter refinement in the MIR and MAD methods. *Methods Enzymol* **276:** 472–494

Esteban PF, Yoon HY, Becker J, Dorsey SG, Caprari P, Palko ME, Coppola V, Saragovi HU, Randazzo PA, Tessarollo L (2006) A kinase-deficient TrkC receptor isoform activates Arf6–Rac1 signaling through the scaffold protein tamalin. *J Cell Biol* **173:** 291–299

Fagni L, Ango F, Perroy J, Bockaert J (2004) Identification and functional roles of metabotropic glutamate receptor-interacting proteins. *Semin Cell Dev Biol* **15:** 289–298

Feng W, Long JF, Fan JS, Suetake T, Zhang M (2004) The tetrameric L27 domain complex as an organization platform for supramolecular assemblies. *Nat Struct Mol Biol* **11:** 475–480

Hall RA, Lefkowitz RJ (2002) Regulation of G protein-coupled receptor signaling by scaffold proteins. *Circ Res* **91:** 672–680

Hillier BJ, Christopherson KS, Prehoda KE, Bredt DS, Lim WA (1999) Unexpected modes of PDZ domain scaffolding revealed by structure of nNOS-syntrophin complex. *Science* **284:** 812–815

Hirose M, Kitano J, Nakajima Y, Moriyoshi K, Yanagi S, Yamamura H, Muto T, Jingami H, Nakanishi S (2004) Phosphorylation and

recruitment of Syk by immunoreceptor tyrosine-based activation motif-based phosphorylation of Tamalin. *J Biol Chem* **279:** 32308–32315

Hung AY, Sheng M (2002) PDZ domains: structural modules for protein complex assembly. *J Biol Chem* **277:** 5699–5702

Im YJ, Lee JH, Park SH, Park SJ, Rho SH, Kang GB, Kim E, Eom SH (2003a) Crystal structure of the Shank PDZ–ligand complex reveals a class I PDZ interaction and a novel PDZ–PDZ dimerization. *J Biol Chem* **278:** 48099–48104

Im YJ, Park SH, Rho SH, Lee JH, Kang GB, Sheng M, Kim E, Eom SH (2003b) Crystal structure of GRIP1 PDZ6-peptide complex reveals the structural basis for class II PDZ target recognition and PDZ domain-mediated multimerization. *J Biol Chem* **278:** 8501–8507

Jones TA, Zou JY, Cowan SW, Kjeldgaard M (1991) Improved methods for building protein models in electron density maps and the location of errors in these models. *Acta Crystallogr A* **47** (Part 2)**:** 110–119

Karthikeyan S, Leung T, Ladias JA (2001) Structural basis of the Na^+/H^+ exchanger regulatory factor PDZ1 interaction with the carboxyl-terminal region of the cystic fibrosis transmembrane conductance regulator. *J Biol Chem* **276:** 19683–19686

Kennedy MB (2000) Signal-processing machines at the postsynaptic density. *Science* **290:** 750–754

Kim E, Sheng M (2004) PDZ domain proteins of synapses. *Nat Rev Neurosci* **5:** 771–781

Kitano J, Kimura K, Yamazaki Y, Soda T, Shigemoto R, Nakajima Y, Nakanishi S (2002) Tamalin, a PDZ domain-containing protein, links a protein complex formation of group 1 metabotropic glutamate receptors and the guanine nucleotide exchange factor cytohesins. *J Neurosci* **22:** 1280–1289

Kitano J, Yamazaki Y, Kimura K, Masukado T, Nakajima Y, Nakanishi S (2003) Tamalin is a scaffold protein that interacts with multiple neuronal proteins in distinct modes of protein–protein association. *J Biol Chem* **278:** 14762–14768

Kneussel M (2005) Postsynaptic scaffold proteins at non-synaptic sites. The role of postsynaptic scaffold proteins in motor-protein-receptor complexes. *EMBO Rep* **6:** 22–27

Kunishima N, Shimada Y, Tsuji Y, Sato T, Yamamoto M, Kumasaka T, Nakanishi S, Jingami H, Morikawa K (2000) Structural basis of glutamate recognition by a dimeric metabotropic glutamate receptor. *Nature* **407:** 971–977

Laskowski RA, MacArthur MW, Moss D, Thornton JM (1993) PROCHECK: a program to check the stereochemical quality of protein structures. *J Appl Crystallogr* **26:** 283–291

Lefkowitz RJ, Shenoy SK (2005) Transduction of receptor signals by beta-arrestins. *Science* **308:** 512–517

Li Z, Sheng M (2003) Some assembly required: the development of neuronal synapses. *Nat Rev Mol Cell Biol* **4:** 833–841

Long JF, Feng W, Wang R, Chan LN, Ip FC, Xia J, Ip NY, Zhang M (2005) Autoinhibition of X11/Mint scaffold proteins revealed by the closed conformation of the PDZ tandem. *Nat Struct Mol Biol* **12:** 722–728

Mok H, Shin H, Kim S, Lee JR, Yoon J, Kim E (2002) Association of the kinesin superfamily motor protein KIF1Balpha with postsynaptic density-95 (PSD-95), synapse-associated protein-97, and synaptic scaffolding molecule PSD-95/discs large/zona occludens-1 proteins. *J Neurosci* **22:** 5253–5258

Nevrivy DJ, Peterson VJ, Avram D, Ishmael JE, Hansen SG, Dowell P, Hruby DE, Dawson MI, Leid M (2000) Interaction of GRASP, a protein encoded by a novel retinoic acid-induced gene, with members of the cytohesin family of guanine nucleotide exchange factors. *J Biol Chem* **275:** 16827–16836

Otwinowski Z, Minor W (1997) Processing of X-ray diffraction data collected in oscillation mode. *Method Enzymol* **276:** 307–326

Penkert RR, DiVittorio HM, Prehoda KE (2004) Internal recognition through PDZ domain plasticity in the Par-6–Pals1 complex. *Nat Struct Mol Biol* **11:** 1122–1127

Pufall MA, Graves BJ (2002) Autoinhibitory domains: modular effectors of cellular regulation. *Annu Rev Cell Dev Biol* **18:** 421–462

Shi Y (2004) Caspase activation: revisiting the induced proximity model. *Cell* **117:** 855–858

Tsuji Y, Shimada Y, Takeshita T, Kajimura N, Nomura S, Sekiyama N, Otomo J, Usukura J, Nakanishi S, Jingami H (2000) Cryptic dimer interface and domain organization of the extracellular region of metabotropic glutamate receptor subtype 1. *J Biol Chem* **275:** 28144–28151

Wong HC, Bourdelas A, Krauss A, Lee HJ, Shao Y, Wu D, Mlodzik M, Shi DL, Zheng J (2003) Direct binding of the PDZ domain of Dishevelled to a conserved internal sequence in the C-terminal region of Frizzled. *Mol Cell* **12:** 1251–1260